Nanoscale

Cite this: *Nanoscale*, 2011, **3**, 4078

www.rsc.org/nanoscale

COMMUNICATION

Self-templated synthesis and thermal conductivity investigation for ultrathin perovskite oxide nanowires†

Gautam G. Yadav,[a] Genqiang Zhang,[a] Bo Qiu,[b] Joseph A. Susoreny,[a] Xiulin Ruan[b] and Yue Wu*[a]

Received 15th June 2011, Accepted 1st August 2011
DOI: 10.1039/c1nr10624d

The large thermal conductivity of bulk complex metal oxides such as $SrTiO_3$, $NaCo_2O_4$, and $Ca_3Co_4O_9$ has set a barrier for the improvement of thermoelectric figure of merit and the applications of these materials in high temperature (≥1000 K) thermoelectric energy harvesting and solid-state cooling. Here, we present a self-templated synthesis approach to grow ultrathin $SrTiO_3$ nanowires with an average diameter of 6 nm in large quantity. The thermal conductivity of the bulk pellet made by compressing nanowire powder using spark plasma sintering shows a 64% reduction in thermal conductivity at 1000 K, which agrees well with theoretical modeling.

Substantial progress has been achieved on using thermoelectric materials to convert waste heat into electricity.[1–3] The performance of thermoelectric materials is usually evaluated by the figure of merit (ZT), which is defined as $S^2T/\rho\kappa$ (S: Seebeck coefficient; ρ: electrical resistivity; T: temperature; κ: thermal conductivity). Recent research on nanostructured thermoelectric materials, especially the nanowires, has shown that a significant improvement in ZT could be achieved because of the dramatic reduction of thermal conductivity in nanowires comparing to the bulk materials.[2,3] On the other hand, the thermoelectric energy harvesting from high-grade heat (>1000 K) is dominated by using $Yb_{11}MnSb_{14}$[4] and Si–Ge,[5,6] both of which exhibit a few obvious drawbacks, including the material instability (oxidation or decomposition) at high temperature and high raw material cost due to the use of scarce elements. In contrast, complex metal oxides, such as $SrTiO_3$, $NaCo_2O_4$, and $Ca_3Co_4O_9$,[7–9] are considered much more stable at high temperature in oxidative atmospheres, and thus are particularly suitable for the thermoelectric devices operating at high temperature. However, the ZT of complex oxides[10–14] has been historically too low for most practical applications due to their extremely large thermal conductivity: for $SrTiO_3$, although it has an unusually high power factor (S^2/ρ) of 20 μW cm^{-1} K^{-2}, the thermal conductivity is 10 W m^{-1} K^{-1}, which results in a ZT of only 0.26 at 1000 K. So, the advantageous chemical and structural stability of complex metal oxides, if coupled with well-controlled nanowire structures with finite diameter, could significantly reduce the thermal conductivity by effectively scattering the phonon at the nanowire surface and interface and provide a promising approach to improve the ZT above the state of the art. At the same time, in order for nanowire-based thermoelectric materials to have a real technological impact, a rational yet scalable synthetic approach has to be developed.

Our interest in $SrTiO_3$ is motivated by its high power factor, high temperature stability (melting point above 2000 °C), and its composition made from non-toxic and earth-abundant elements.[7,15] The synthesis of SrTiO3 nanowires has been pursued by several groups, which involve either the synthesis, oxidation, and decomposition of a highly flammable bimetallic alkoxide precursor of strontium titanium isopropoxide[16] or high temperature (>800 °C) solid state reaction between strontium oxalate and TiO_2,[17] yet neither yielded uniform nanowires in large quantity with diameter below 10 nm and narrow size distribution. In this study, we demonstrate the development of rational synthesis of ultrathin $SrTiO_3$ nanowires with an average diameter of 6 nm through a novel self-templated approach and show that indeed the thermal conductivity of the bulk pellet fabricated by compressing these $SrTiO_3$ nanowire powder using spark plasma sintering can be reduced by 64% at 1000 K.

The self-templated synthesis approach involves two steps that can be characterized separately using X-ray diffraction (XRD, Fig. 1a) and transmission electron microscopy (TEM) as shown in Fig. 1b–d. In a typical growth, 0.08 g of TiO_2 nanopowders (anatase, purchased from Aldrich, Fig. 1b) are mixed with 6.8 g potassium hydroxide (KOH) in 12 mL water (H_2O) and heated for 3 days to synthesize potassium titanate ($K_2Ti_8O_{17}$) nanowires (Fig. 1c) in a hydrothermal reactor at 200 °C. These $K_2Ti_8O_{17}$ nanowires, which can be washed and collected as the self templates, will then be re-mixed with 0.106 g strontium nitrate [$Sr(NO_3)_2$] and 0.67 g KOH in 10 mL water and heated for another day in a hydrothermal reactor at the same temperature to obtain $SrTiO_3$ nanowires (Fig. 1d) through the cation exchange reaction.[18] The overall yield of $SrTiO_3$ nanowires is up to 60% estimated from the starting precursors. XRD analysis (Fig. 1a)

[a]*School of Chemical Engineering, Purdue University, West Lafayette, IN, 47907, USA*
[b]*School of Mechanical Engineering, Purdue University, West Lafayette, IN, 47907, USA. E-mail: yuewu@purdue.edu; Fax: +1 765-494-0805; Tel: +1 765-494-6028*

† Y. Wu thanks the support from the Purdue University new faculty startup grant, Kick Grant from Birck Nanotechnology Center, DuPont Young Faculty Award, Midwest Institute for Nanoelectronics Discovery (MIND), and NSF/DOE Thermoelectric Partnership (Award Number 1048616). Y. Wu acknowledges the help from Dr Douglas Dudis and Charles Cooke at Wright-Patterson Air Force Research Lab on the spark plasma sintering of nanowire powder. X.L. Ruan and B. Qiu acknowledge the partial support of Air Force Office of Scientific Research (Grant Number FA9550-11-1-0057).

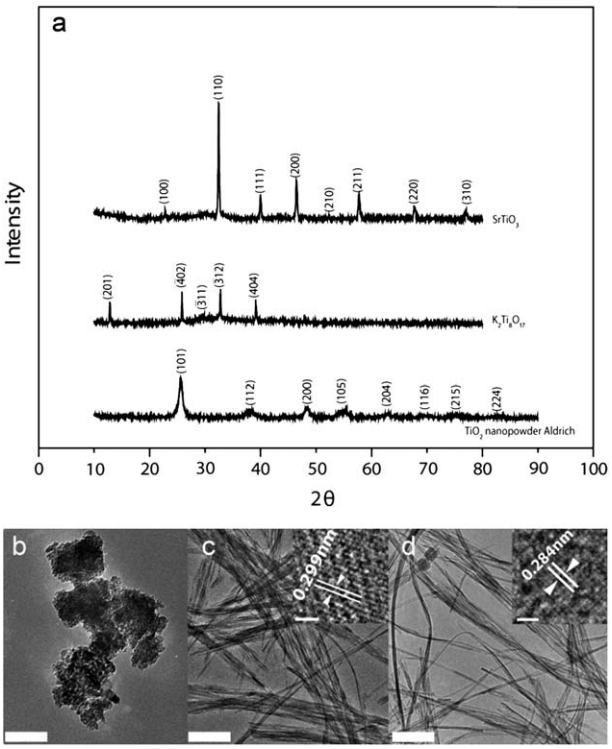

Fig. 1 (a) XRD patterns of $SrTiO_3$, $K_2Ti_8O_{17}$ and TiO_2 nanopowder Aldrich, respectively. (b) TEM image of TiO_2 nanopowder Aldrich (scale bar, 50 nm). (c) TEM image of $K_2Ti_8O_{17}$ nanowires (scale bar, 100 nm), inset at the top corner is a HRTEM image of a $K_2Ti_8O_{17}$ nanowire (scale bar, 2 nm). (d) TEM image of $SrTiO_3$ nanowires (scale bar, 100 nm), inset at the top corner is a HRTEM image of a $SrTiO_3$ nanowire (scale bar, 2 nm).

confirms the full conversion from TiO_2 to $SrTiO_3$ through the intermediate step of $K_2Ti_8O_{17}$. Low magnification TEM characterizations show that both $K_2Ti_8O_{17}$ (Fig. 1c) and $SrTiO_3$ (Fig. 1d) nanowires have very narrow diameter distribution with an average diameter of 6.79 ± 1.18 nm for $K_2Ti_8O_{17}$ and 5.8 ± 0.89 nm for $SrTiO_3$, respectively. Notably, both $K_2Ti_8O_{17}$ (Fig. 1c) and $SrTiO_3$ (Fig. 1d) nanowires tend to bundle together due to the lack of organic capping ligands while surprisingly maintaining as a stable suspension in water without the overgrowth even after a four-day process, which is mainly due to the colloidal behaviour associated with their finite diameters. High resolution TEM (HRTEM) characterizations have also been used to characterize the crystallinity of our nanowires, which indicate that both $K_2Ti_8O_{17}$ (inset, Fig. 1b) and $SrTiO_3$ (inset, Fig. 1c) nanowires are single crystals and the lattice fringes in the HRTEM images have been identified as $(\bar{3}11)$ and (110) for $K_2Ti_8O_{17}$ and $SrTiO_3$, respectively.

The uniform $SrTiO_3$ nanowires with diameters less than 10 nm could significantly increase the scattering of phonons at the nanowire surface and interface, thus reducing the thermal conductivity.[19,20] In order to measure the thermal conductivity of the ultrathin $SrTiO_3$ nanowires, we have fabricated bulk pellets of $SrTiO_3$ nanowires with 1 inch diameter and 0.1 inch thickness by performing spark plasma sintering (SPS) on the dried nanowire powders. The large DC current (15 KA) and high pressure (50 MPa) have helped to obtain a relative density of 54.4% within 10 minutes of sintering at 800 K. Thermal diffusivity measurements have been performed on these pellet samples, which show a slightly increased thermal conductivity from room temperature to 1000 K with a value of 1.95 W m^{-1} K^{-1} at 1000 K (Fig. 2, blue triangles).

In order to understand the reduction of the thermal conductivity in these ultrathin nanowires and its temperature dependence, we use an effective porous medium approximation together with empirical fitting. In the prepared sample, the electronic carrier concentration is relatively low so that the electronic contribution to the thermal conductivity can be neglected, and the thermal conductivity is solely contributed by phonons. In $SrTiO_3$ bulk crystals, phonon transport is dominated by phonon–phonon scattering. However, in the SPS-processed sample the $SrTiO_3$ nanowires are randomly oriented and interconnected, and phonons are mainly transported along 1D nanowires and across nanowire–nanowire contacts. Therefore, intrinsic phonon–phonon scattering is no longer important while phonon scattering at nanowire surfaces and contacts become essential. We note that the value of interfacial thermal resistance is typically in the order of 10^{-9} to 10^{-7} m^2 K W^{-1}.[21–23] In the case of $SrTiO_3$ nanowires with a diameter of 6 nm, the interfacial contact area between two interconnected nanowires can be assumed to be 3×10^{-17} m^2 or larger, and the associated thermal contact resistance is about 10^7 to 10^9 K W^{-1}. On the other hand, the typical length of our $SrTiO_3$ nanowires is around 100 nm, and if we assume the thermal conductivity of an individual $SrTiO_3$ nanowire to be 2 W m^{-1} K^{-1}, the corresponding nanowire axial thermal resistance is about 10^9 to 10^{10} K W^{-1}. As we can see, the contact thermal resistance is generally lower than that of nanowire axial resistance and is unimportant when arranged in series. Therefore, as a good approximation, the thermal resistance of nanowire contacts is neglected at the moment. Under such simplifications, nanowire composite can be viewed as a continuous porous medium, with the "solid" to be interconnected $SrTiO_3$ nanowires and the "pores" to be the air gaps. Since the thermal conductivity of air is very low, the relationship between the effective thermal conductivity of the nanoporous medium and that of unperturbed continuous medium can be obtained as:[24]

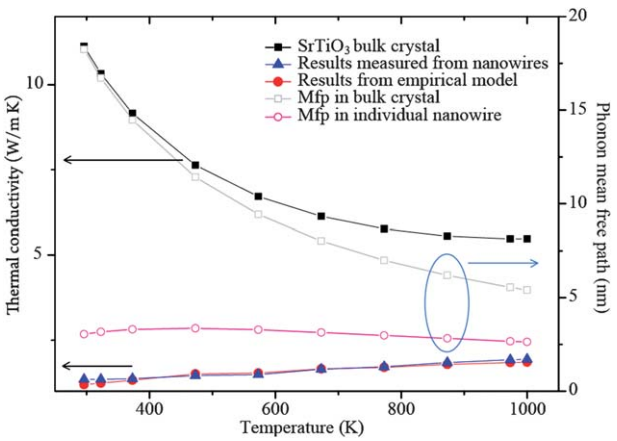

Fig. 2 Comparison of thermal conductivity plot between bulk crystal data (extrapolated from ref. 29), empirical model and experimental measurements of SrTiO3 nanowires. Also presented are the effective phonon mean free paths (Mfp) in bulk crystal and SrTiO3 individual nanowires.

$$k_{eff}/k_0 = (1 - P)^{3/2},$$

where k_{eff} is the effective thermal conductivity of nanocomposite and k_0 is the average thermal conductivity of an individual nanowire. $P = (\rho - \rho_{eff})/\rho = 0.46$ is the porosity, where $\rho = 5.13$ g cm^{-3} is the $SrTiO_3$ bulk density and $\rho_{eff} = 2.787$ g cm^{-3} is the measured density of our sample. The parameter e is the shape factor of pores and is taken to be 2/3 to account for the fully random shapes of the air gaps. We can reach a simple relation between k_{eff} and k_0:

$$k_{eff} = 0.543k_0 \quad (1)$$

To interpret the measured thermal conductivity, we use an empirical model which takes into account the temperature dependence of thermal conductivity:[25,26]

$$\frac{\kappa_0(T)}{c_0(T)} = \frac{\kappa_b(T)}{c_b(T)} p \exp\left(-\alpha \frac{l_b(T)}{D}\right)\left(-\frac{\beta}{D/L - 1}\right)^{3/2} \quad (2)$$

where c is the specific heat, p is the specularity parameter ranging from 0 to 1, $l_b = l_r T_r/T$ is the temperature-dependent mean free path, $D = 6$ nm is the nanowire diameter, $L = 1.1$ nm is the critical size at which almost all atoms are localized at the nanowire surface. $\alpha = 0.5$ is a geometrical factor. β is related to melting entropy and is kept as an adjustable parameter since no experimental data is available. Here the subscripts "0", "b", "r" indicate "nanowire", "bulk", and "reference", respectively. The bulk specific heat data are extrapolated from ref. 27. The bulk mean free path at $T_r = 300$ K is estimated to be $l_r = 18$ nm by comparing to that of Bi_2Te_3 since simple calculation from kinetic theory is found to severely underestimate the effective mean free path.[28]

The best fitting to the measurement data of $SrTiO_3$ nanowires thermal conductivity is achieved with parameters $p = 1.0$, and $\beta = 1.2$. The results are shown in Fig. 2 in comparison with the measured data (Fig. 2, blue triangle), in which the black squares correspond to the bulk crystals and the red circles correspond to the nanowires. It is seen that the agreement is excellent for the entire temperature range. The slight underestimation in the modeled thermal conductivity at higher temperatures is likely due to the alleviation of defects and better thermal contacts among nanowires at high temperatures, which will lead to an apparent increase in the mean free path and in turn lead to higher thermal conductivity values. The fitted sound velocity is 4800 m s^{-1}, which is smaller than the corresponding bulk value (5500 m s^{-1} in average).[30] This is a result of the phonon-softening phenomenon originated from the altered atomic vibrations at thin nanowire surfaces.[26] On the other hand, as also seen in Fig. 2, the phonon mean free paths in individual nanowires (pink circles) are found to be only weakly dependent on temperature with values much less than those in bulk (gray squares). Such observation indicates that, due to the very small diameters, strong phonon scattering at nanowire surfaces dominates over the Umklapp scattering and greatly limits the effective mean free path. Also, the temperature-insensitive nature of such scattering leads to the weak temperature dependence of mean free paths in $SrTiO_3$ nanowires. Therefore, the trend that thermal conductivity slowly increases with temperature can be attributed to the weak temperature dependence in mean free path, and the increase in the measured specific heat with temperature due to the relatively high Debye temperature of $SrTiO_3$ (513 K).[31] From the analysis, it can be summarized that boundary scattering contributes to about 45% (at 1000 K) to 85% (at 300 K) reduction to thermal conductivity, while the porosity contributes to an additional 45% percent reduction. The former mechanism will not affect electrical conductivity much since electrons have much shorter intrinsic mean free paths, indicating a potential for significant ZT enhancement.

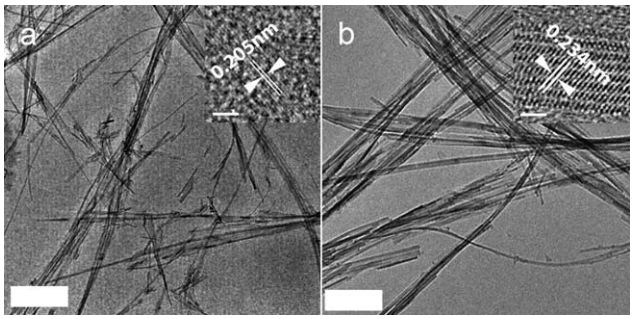

Fig. 3 (a) TEM image of $BaTiO_3$ nanowires (scale bar, 0.2 μm), inset at the top corner is the HRTEM image of $BaTiO_3$ nanowire (scale bar, 5 nm). (b) TEM image of $PbTiO_3$ nanowires (scale bar, 100 nm), inset at the top corner is the HRTEM image of $PbTiO_3$ nanowire (scale bar, 2 nm).

In addition, our self-templated synthesis approach can also be used to grow other perovskite nanowires, for example barium titanate ($BaTiO_3$, Fig. 3a) and lead titanate ($PbTiO_3$, Fig. 3b), by replacing Sr $(NO_3)_2$ with 0.131 g barium nitrate [$Ba(NO_3)_2$] and 0.166 g lead nitrate [$Pb(NO_3)_2$]. These nanowires also exhibit finite diameters of 8.15 ± 1.35 nm and 9.49 ± 1.48 nm for $BaTiO_3$ and $PbTiO_3$, respectively. The generality of this synthetic approach could enable us to further explore the thermoelectric properties of the complicated layered perovskite nanowires by mixing various cation precursors. These complicated layered perovskites, which have a general formula of $M_m[A_{n-m}B_nO_{3n+1}$ (M = Cs, Rb, K, Na, Li, *etc.*; A = Ba, Sr, Ca, rare earth, *etc.*; B = Ti, Nb, Ta, W, Mo, *etc.*), can exist in either Dion–Jacobson ($m = 1$) or Ruddlesden–Popper ($m = 2$) phases and are consisted of perovskite-like slabs (n = layers of the perovskite-like slab) and interlayers. These layered structures can be regarded as natural superlattices with the perovskite-like slabs and the interlayers in the superlattices to be tuned independently to generate a specific function to optimize electron transport. The sublattice interfaces are also expected to enhance the phonon scattering to further suppress the thermal conductivity and improve the thermoelectric performance.[32]

In conclusion, we have demonstrated that a facile self-templated hydrothermal synthesis method can be used for the preparation of ultrathin perovskite oxide nanowires. These nanowires, using $SrTiO_3$ as an example, exhibit a significantly reduced thermal conductivity, which opens the possibility to improve the thermoelectric performance of these non-toxic and abundant metal oxide-based materials as alternations for skutterudites and Si/Ge for high temperature energy harvesting and solid-state cooling.

Notes and references

1 D. Y. Chung, M. G. Kanatzidis and J. S. Sootsman, *Angew. Chem., Int. Ed.*, 2009, **48**, 8616–8639.
2 R. Chen, R. D. Delgado, E. C. Garnett, A. I. Hochbaum, W. Liang, A. Majumdar, M. Najarian and P. Yang, *Nature*, 2008, **451**, 734–167.
3 A. I. Boukai, Y. Bunimovich, W. A. Goddard, J. R. Heath, J. T. Kheli and J. K. Yu, *Nature*, 2008, **451**, 168–171.
4 S. R. Brown, F. Gascoin, S. M. Kauzlarich and G. J. Snyder, *Chem. Mater.*, 2006, **18**, 1873.
5 C. Wood, *Energy Convers. Manage.*, 1984, **24**, 331.

6 J. Sadatomi and O. Yamashita, *J. Appl. Phys.*, 2000, **88**, 245.
7 R. Funahashi, K. Koumoto and I. Terasaki, *MRS Bull.*, 2006, **31**, 206.
8 Y. Sasago, I. Terasaki and K. Uchinokura, *Phys. Rev. B: Condens. Matter*, 1997, **56**, R12685.
9 J. F. Li, J. Li, D. Liu, F. Ma, Y. Ou, S. Xie and T. Yin, *J. Phys. Chem. C*, 2010, **114**, 10061.
10 M. Hirano, H. Hosono, K. Koumoto, H. Ohta and S. Ohta, in Extended Abstracts No. 1 of the 52nd Spring Meeting, Jpn. Soc. Appl. Phys. Related Soc., 2005, p. 254.
11 E. Maed, Y. Nojiri and M. Ohtaki, *Proc. 19th Int. Conf. Thermoelectrics*, IEEE, Wales, 2000, p. 190.
12 I. Terasaki, *Proc. 21st Int. Conf. Thermoelectrics*, 2002, p. 185.
13 K. Fujita, T. Mochida and K. Nakamura, *Jpn. J. Appl. Phys.*, 2001, **40**, 4644.
14 D. Chateigner, K. Chong, R. Funahashi, E. Guilmeau and M. Mikami, *Appl. Phys. Lett.*, 2004, **85**, 1490.
15 Strontium Titanate, Product No. 517011[Online], Sigma-Aldrich: Saint Louis, MO, July 20, 2010, http://simaaldrich.com/catalog/ProductDetail.do?lang=en&N4=517011|ALDRICH&N5=SEARCH_CONCAT_PNO|BRAND_KEY&f=SPEC, accessed May 16 2011.
16 J. J. Urban, W. S. Yun, Q. Gu and H. Park, *J. Am. Chem. Soc.*, 2002, **124**, 1186–1187.
17 S. Banerjee, Y. Mao and S. S. Wong, *J. Am. Chem. Soc.*, 2003, **125**, 15718–15719.
18 D. H. Son, S. M. Hughes, Y. Yin and A. P. Alivisatos, *Science*, 2004, **306**, 1009–1012.
19 G. Chen, M. S. Dresselhaus, J. P. Fleurial, P. Gogna, H. Lee, Z. Ren, M. Tang, D. Wang and R. Yang, *Adv. Mater.*, 2007, **19**, 1043–1053.
20 R. Yang and G. Chen, *Phys. Rev. B: Condens. Matter Mater. Phys.*, 2004, **69**, 195316.
21 S. T. Huxtable, D. G. Cahill, S. Shenogin, L. Xue, R. Ozisik, P. Barone, M. Usrey, M. S. Strano, G. Siddons, M. Shim and P. Keblinski, *Nat. Mater.*, 2003, **2**, 731.
22 H. Lyeo and D. G. Cahill, *Phys. Rev. B: Condens. Matter Mater. Phys.*, 2006, **73**, 144301.
23 B. C. Grundum, D. G. Cahill and R. S. Averback, *Phys. Rev. B: Condens. MatterMater. Phys.*, 2005, **72**, 245426.
24 T. H. Bauer, *Int. J. Heat Mass Transfer*, 1993, **36**, 4181.
25 L. H. Liang and B. Li, *Phys. Rev. B: Condens. Matter Mater. Phys.*, 2006, **73**, 153303.
26 B. Qiu, L. Sun and X. Ruan, *Phys. Rev. B: Condens. Matter Mater. Phys.*, 2011, **83**, 035312.
27 D. de Ligny and P. Richet, *Phys. Rev. B: Condens. Matter*, 1996, **53**, 3013.
28 C. Jeong, S. Datta, and M. Lundstrom, *J. Appl. Phys.*, 2011, **109**, 073718.
29 H. Muta, K. Kurosaki, and S. Yamanaka, *J. Alloys Compd.*, 2005, **392**, 306.
30 R. O. Bell and G. Rupprecht, *Phys. Rev.*, 1963, **129**, 90.
31 M. Ahrens, R. Merkle, J. Maier and B. Rahmati, *Phys. B*, 2007, **393**, 239.
32 R. E. Schaak and T. E. Mallouk, *Chem. Mater.*, 2002, **14**, 1455–1471.